

Magnetic Resonance Perfusion-Weighted Imaging of Acute Cerebral Infarction

Effect of the Calculation Methods and Underlying Vasculopathy

Kei Yamada, MD; Ona Wu, MS; R. Gilberto Gonzalez, MD, PhD; Dirk Bakker, MD; Leif Østergaard, MD, MSc; William A. Copen, MS; Robert M. Weisskoff, PhD; Bruce R. Rosen, MD, PhD; Katsumi Yagi, PhD; Tsunehiko Nishimura, MD, PhD; A. Gregory Sorensen, MD

Background and Purpose—Various calculation methods are available to estimate the transit-time on MR perfusion-weighted imaging (PWI). Each method may affect the results of PWI. Steno-occlusive disease in the parent vessels is another factor that may affect the results of the PWI. The purpose of this study was to elucidate the effect of the calculation methods and underlying vasculopathy on PWI.

Methods—From a pool of 113 patients who had undergone PWI during the study period, a total of 12 patients with nonlacunar ischemic strokes who were scanned within 24 hours after onset of symptom were selected for the study. The patient population consisted of 6 patients who had extracranial internal carotid artery stenosis (>70%) and 6 individuals without stenosis. Seven different postprocessing methods were evaluated: first moment, ratio of area to peak, time to peak (TTP), relative TTP, arrival time, full-width at half-maximum, and deconvolution methods. Follow-up MR or CT images were used to determine the areas that evolved into infarcts, which served as the gold standard. Sensitivity and specificity of each transit time technique were calculated.

Results—Calculation methods with high sensitivity were the first moment (sensitivity, 74%), TTP (sensitivity, 77%), and deconvolution methods (sensitivity, 81% to 94%). Between the 2 groups with and without internal carotid artery stenosis, the specificity of most of the techniques was lower in the internal carotid artery stenosis group. The first moment and deconvolution methods maintained relatively high specificity even in the stenosis group.

Conclusions—The calculation technique and presence of underlying vasculopathy have a direct impact on the results of PWI. The methods with high sensitivity even in the presence of steno-occlusive disease were the first moment and deconvolution methods with arterial input function derived from the peri-infarct arteries; the deconvolution method was the superior choice because of higher lesion conspicuity. (*Stroke*. 2002;33:87-94.)

Key Words: brain ■ diffusion ■ magnetic resonance imaging ■ perfusion ■ stroke, acute

Although conventional CT imaging and MR imaging are excellent modalities for detecting and characterizing cerebral ischemia or infarction, they may fail to depict acute ischemia reliably at its earliest stage.¹ One of the most useful methods currently available is MR diffusion-weighted imaging (DWI), which may also underestimate the final size of the infarct when performed within the first day.² In the acute stage of stroke, therefore, it has been shown that DWI, combined with measures of cerebral hemodynamics, may be beneficial in the estimation of the surrounding area of ischemic tissue at risk, the so-called ischemic penumbra.²

Dynamic susceptibility contrast imaging is one of the most commonly used techniques for obtaining MR perfusion-

weighted images (PWI).²⁻⁹ A series of T2*-weighted images is acquired during the transit of a bolus of contrast material through the brain. The recorded signal intensity-time curves are converted to concentration-time curves for calculation of the perfusion parameters. Among the various hemodynamic parameters, such as cerebral blood flow and cerebral blood volume, the ones that reflect transit time (eg, mean transit time) are most commonly used to estimate perfusion deficits in acute stroke patients. This is based in part on the well-known immediate coupling of mean transit time (MTT) with cerebral perfusion pressure.^{10,11} In addition, transit time parameters are able to delineate the visually distinct regions of abnormality^{12,13} and the perfusion deficits of greater

Received April 26, 2001; final revision received July 12, 2001; accepted September 20, 2001.

From the Massachusetts General Hospital NMR Center, Harvard Medical School, Boston (K.Y., O.W., R.G.G., D.B., W.A.C., R.M.W., B.R.R., A.G.S.); Departments of Radiology (K.Y., T.N.) and Mathematics (K.Y.), Kyoto Prefectural University of Medicine, Kyoto, Japan; and Department of Neuroradiology, Aarhus University Hospitals, Aarhus, Denmark (L.Ø.).

Reprints requests to Kei Yamada, Department of Radiology, Kyoto Prefectural University of Medicine, Kajii-cho, Kawaramachi Hirokoji Sagaru, Kamigyo-ku, Kyoto City, Kyoto, Japan 602-8566. E-mail kyamada@koto.kpu-m.ac.jp

© 2002 American Heart Association, Inc.

Stroke is available at <http://www.strokeaha.org>

volume compared with the cerebral blood flow or cerebral blood volume maps, which suggests that they are more representative of the maximum anatomic extent of perfusion impairment.¹²

Various ways have been proposed to estimate transit time, including ratio of area to peak,^{14,15} first moment,^{12,15-19} deconvolution,^{9,20,21} time to peak (TTP),^{13,22,23} time of the contrast arrival (arrival time),²⁴ and relative TTP (TTP minus arrival time).²⁴ The first 3 calculation techniques estimate the true MTT; the last 4 techniques are surrogate measures that may simulate the mean transit time. Although all of these techniques have already been accepted as part of routine clinical practice, the differences in their ability to determine the areas of perfusion deficit have not been fully addressed. To the best of our knowledge, no studies have done a systematic comparison of these various transit time calculation techniques using a single set of perfusion data. Without knowledge of the general trends and limitations of these various postprocessing techniques, the true efficacy of the PWI is difficult to assess. Thus, the first purpose of this paper was to compare these various calculation methodologies and to determine the transit time calculation method that is most suited for the imaging of acute stroke patients.

The second purpose of this study was to evaluate the effect of major vasculopathy involving the parent arteries of the brain. Steno-occlusive disease in the parent vessels may cause significant delay or distortion of the peak of the concentration-time curves. It is apparent, however, that the degree of curve distortion may not be directly correlated with local hemodynamic status, because the perfusion of brain tissue is dependent on many factors other than the degree of stenosis, which may include collaterals via the circle of Willis and leptomeningeal anastomoses. Thus, it can be predicted that the presence of steno-occlusive disease will result in false-positive depictions of regional flow deficit. Underlying vasculopathy may have a different degree of influence on each calculation technique, and thus our second purpose was to elucidate the effect of steno-occlusive disease on the results of PWI. In this study, we specifically focused on steno-occlusive disease of the internal carotid artery (ICA) to simplify the study design.

Materials and Methods

Patients

A retrospective search of the neuroradiology report database system our institution covering November 1995 through December 1997 revealed 113 patients who had undergone PWI studies. Within this patient population, 6 cases met the following inclusion criteria: (1) patients with acute nonlacunar ischemic stroke involving the cerebral cortex; (2) PWI performed within 24 hours after the onset of ictus; (3) availability of follow-up imaging studies, either MR or CT, that allowed determination of the final area of the infarction; and finally (4) stenosis of the ipsilateral extracranial ICA >70%. The ICA stenoses were due to atherosclerotic disease (n=3), embolism (n=1), dissection (n=1), or balloon embolization for treatment of giant cavernous aneurysm (n=1). Location and severity of the ICA stenoses were confirmed by 2 modalities in each case, which included conventional angiogram (n=2), ultrasonography (n=3), CT angiogram (n=2), and MR angiogram (n=5). All of these ICA stenoses were noted on the side of acute infarctions. The steno-occlusive disease of other vessels, including the contralateral ICA,

was not present in any of the selected cases. The age of these patients ranged from 33 to 80 years (mean, 66.7 years).

Six patients with acute cerebral infarction but without ICA vasculopathy were randomly selected from a pool of PWI studies performed during the same study period. The inclusion criteria were as follows: (1) acute nonlacunar ischemic stroke involving the cortex, (2) PWI performed within 24 hours, (3) follow-up studies, and (4) absence of carotid stenosis. These cases were determined to be negative for ICA vasculopathy from MR angiogram (n=6) and CT angiogram (n=1). The age of these patients ranged from 45 to 72 years (mean, 63.8 years). None of these patients had experienced reperfusion or recanalization. None of these 12 patients had undergone aggressive interventions, such as intra-arterial thrombolysis or recombinant tissue plasminogen activator administration. The study was approved by an institutional review committee, and informed consent was obtained from all patients or their next of kin.

MR Technique

The MR images were obtained with a GE Signa 1.5-T imager (GE Medical Systems) retrofitted for echo-planar imaging (EPI) capabilities (Instascan, Advanced NMR Systems). The PWIs were obtained as part of our standard protocol for stroke patients.² The PWIs were obtained with a single-shot, spin-echo EPI sequence (n=7) or a gradient-echo EPI sequence (n=5). The EPI sequence was a resistance time of 1500 ms, an echo time of 50/75 ms (gradient echo/spin echo, respectively), and a flip angle of 90°. We obtained 46 images in each of 11 sections. Slice thickness and interslice gaps were 6 and 1 mm, respectively. A 256×128 acquisition matrix was used with a 40×20-cm field of view, leading to a pixel size of 1.6×1.6 mm. Injected gadopentetate dimeglumine (Magnevist, Berlex Laboratories) was 0.2 mmol/kg body weight. Contrast was injected 10 seconds after the start of imaging at a rate of 5 mL/s with the use of an MRI-compatible power injector (Medrad). The bolus of contrast material was followed by a similar volume of normal saline, which was also injected at a rate of 5 mL/s.

PWI Calculation

Obtained EPIs were processed to create the various PWIs. Three different calculation methods were used to compute MTT: first moment,²⁵ ratio of area to peak,¹⁵ and deconvolution methods.²⁰ A detailed discussion of the deconvolution technique is provided elsewhere.^{20,21} In brief, the concentration of intravascular contrast agent within a given volume of interest (VOI) can be expressed by $CVOI(t) = Ft \times \int_0^t Ca(\tau)R(t-\tau)d\tau$, where Ft is tissue flow, $Ca(\tau)$ is the arterial input function (AIF), and $R(t)$ is the vascular residue function describing the fraction of tracer still present in the vascular bed of the VOI at time t after injection of contrast. Residue function and flow can be calculated when the concentration-time curve [CVOI(t)] and AIFs [Ca(τ)] are given. An AIF is obtained by choosing 7 to 15 pixels adjacent to the artery with early and large drop in signal intensity (3 to 10 times that of gray and white matter). The concentration-time curves of these pixels were averaged to yield a good representation of arterial contrast levels (Figure 1). These AIFs were chosen by 1 of the authors (K.Y.). AIFs can be chosen from any artery in a certain slice of an axial image. Multiple AIFs were systematically selected from 4 different locations in each subject and computed 4 different PWIs with the deconvolution technique. The arteries used for AIFs included (1) the M1 segment of the ipsilateral middle cerebral artery (MCA), (2) the M1 segment of the contralateral MCA, (3) the P1/P2 segments of the posterior cerebral arteries (PCAs), and (4) the small arteries in the peripheral region of the ischemic/infarcted volume demonstrated on DWI.

In addition to these calculation methods, other surrogate parameters empirically known to be useful for perfusion estimates were also examined. These included TTP, arrival time, relative time to peak (TTP minus arrival time), and full-width at half-maximum (FWHM) (Figure 2).

Data Analysis

Interobserver reliability was tested between 2 fully trained neuroradiologists (D.B., K.Y.). Individual PWI calculated by each postpro-

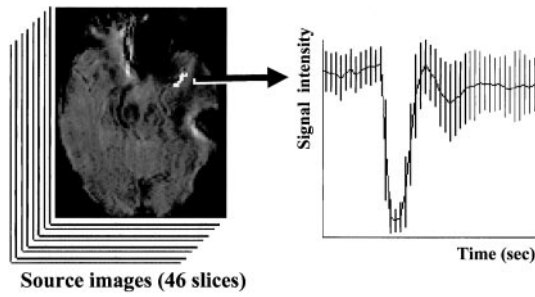


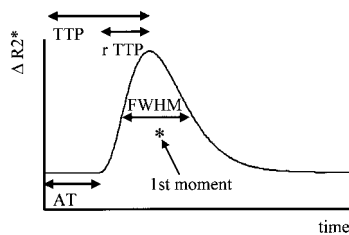
Figure 1. AIFs were chosen directly from the echo-planar source images by selecting 7 to 15 pixels adjacent to the artery with an early and large drop in signal intensity. These pixels were averaged to yield a good representation of arterial contrast levels. Error bars on the signal intensity–time curve represent ± 1 SD of the averaged signal intensity.

cessing method was shown to the readers in a random order. The readers were blinded with respect to the history and final extent of infarction demonstrated on the follow-up scans.

All 11 slices of PWIs were shown to the readers on a workstation screen. The readers were instructed to describe the extent of the area of abnormality according to predetermined brain segments (Figure 3). This template of brain segments was designed to make the reader’s description as specific as possible. Each hemisphere of the brain was divided into 14 segments based on vascular territories. The brain segments consisted of MCA superior division, MCA inferior division, anterior cerebral artery, and PCA, as well as the end-artery territories arising from the anterior and posterior circulations that were arbitrarily named lenticulostriate and thalamoperforator territories, respectively. Each of the above-mentioned 2 segments of the MCA territory was further divided into anterior and posterior parts to make the description more specific. Furthermore, the major vascular territories (excluding the lenticulostriate and thalamoperforator) were also subdivided into cortical and subcortical regions.

After this initial reading session and on a separate day, the follow-up MR (including the DWI) and/or CT images and the initial DWI of each case were shown to the reader in a random fashion. Once again, the reader was instructed to assign the regions of abnormality on the above-mentioned template, and this served as the gold standard. These follow-up scans were obtained between 3 and 16 days (mean, 6.6 days) after the initial PWI.

If an abnormality depicted on PWI was confirmed to have evolved into an infarction on the follow-up scan, it was judged that this was a true-positive result for infarct depiction. If there was an area of PWI abnormality that failed to evolve into true infarct on the follow-up scan, the PWI was judged false-positive (Figure 3). These rates of matching and mismatching between the PWIs and follow-up scans were examined for sensitivity, specificity, negative predictive



1st moment: first moment (center of gravity)
 TTP: time to peak
 rTTP: relative time to peak
 FWHM: full width half maximum
 AT: arrival time

Figure 2. Typical shape of a concentration-time curve is shown with the various parameters used for transit time estimation. AT indicates arrival time; 1st moment, first moment (center of gravity); and rTTP, relative TTP.

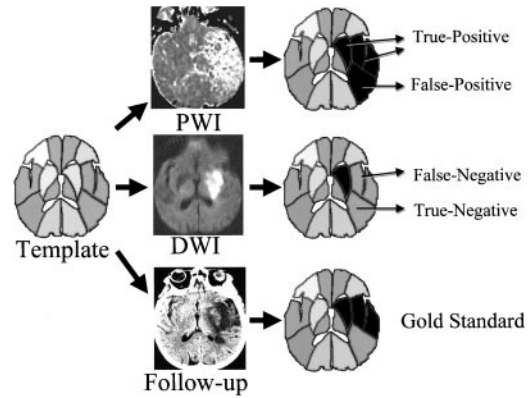


Figure 3. Schematic of the brain template and image analysis process is demonstrated. Representative slice through the basal ganglia is shown. Areas of signal abnormality on DWI, PWI, and follow-up studies were assigned to the predetermined brain template that is based on the vascular territory. Brain segments that had abnormality on PWI that evolved into an area of infarct on follow-up studies were judged true-positive. Brain segments that did not have abnormality on PWI but were found to have evolved into true infarcts were judged false-negative.

values (NPV), positive predictive values (PPV), and accuracy calculation.

Statistical Analysis

Interobserver agreements were assessed by calculating the Cohen coefficient. Agreements were classified as mild (Cohen’s coefficient >0.40), good (>0.60), or excellent (>0.80). The differences in sensitivity, specificity, NPV, PPV and accuracy between the DWI and each calculation method were performed by use of χ^2 analysis of Steel’s method, which is a nonparametric modification of a multiple comparison procedure of Dunnett’s method. Differences between the stenosis and nonstenosis groups were tested with χ^2 analyses. Differences with a value of $P < 0.05$ were regarded as statistically significant.

Results

Good interobserver agreement was noted between the 2 readers (Cohen’s coefficient, 0.68; 95% CI, 0.64 to 0.72). Because the Cohen’s coefficient indicated substantial correlation between 2 observers, data from the second reader were used for the subsequent analysis.

Effect of Calculation Methods

The sensitivity, specificity, PPV, NPV, and accuracy of each PWI calculation technique for all 12 patients are shown in Table 1. The sensitivity and specificity values of the DWI obtained at the time of PWI are given in the top row as reference. As shown in Table 1, the DWI has high specificity (98%), PPV (93%), NPV (86%), and accuracy (88%) but relatively low sensitivity (60%). Thus, the primary role of PWI may be to supplement the relatively low sensitivity of DWI.

Calculation methods of PWI with high sensitivity include MTT images calculated by deconvolution (sensitivity; 81% to 94%), TTP (sensitivity; 77%), and the first moment method (sensitivity; 74%), all of which have higher sensitivity than DWI (sensitivity; 60%). Among these calculation methods, statistically significant differences with DWI ($P < 0.05$) were noted for the deconvolution methods with AIF from contralateral MCA, ipsilateral MCA, and PCA. Figure 4A and 4B

TABLE 1. Sensitivity, Specificity, PPV, NPV, and Accuracy of Each PWI Calculation Technique

	Sensitivity, %	Specificity, %	PPV, %	NPV, %	Accuracy, %
DWI	60 (46-74)	98 (96-100)	93 (84-100)	86 (80-92)	88 (82-93)
First moment	74 (62-87)	84† (78-91)	65† (52-78)	89 (84-95)	82 (76-87)
Area to peak	40 (26-54)	94 (90-98)	73 (56-90)	80 (74-87)	79 (73-85)
Deconvolution (contralateral MCA)	94* (87-100)	69† (61-78)	54† (43-65)	97* (93-100)	76† (70-83)
Deconvolution (ipsilateral MCA)	87* (78-97)	79† (71-86)	61† (50-73)	94 (89-99)	81 (75-87)
Deconvolution (PCA)	85* (75-95)	79† (71-86)	61† (49-72)	93 (88-98)	80 (74-86)
Deconvolution (peri-infarct)	81 (70-92)	92 (87-97)	79 (68-91)	93 (88-97)	89 (84-93)
FWHM	51 (37-65)	93 (88-97)	73 (58-88)	83 (77-89)	81 (75-87)
TTP	77 (64-89)	79† (71-86)	58† (46-70)	90 (84-95)	78 (72-84)
rTTP	64 (50-78)	86† (80-92)	64† (50-78)	86 (80-92)	80 (74-86)
Arrival time	51 (37-65)	90 (85-95)	67 (51-82)	83 (76-89)	79 (73-85)

Numbers in parentheses are the 95% CI.

* $P < 0.05$ higher than DWI; † $P < 0.05$ lower than DWI.

show sensitivity versus specificity and NPV versus PPV, respectively. The calculation methods closer to the upper right corner are considered the ideal calculation methods. In this regard, the deconvolution method with AIF from peri-infarct arteries appeared to be one of the best calculation methods. The relative TTP, ratio of area to peak, FWHM, and arrival time image had sensitivities not significantly different from or inferior to the DWI (sensitivity; 40% to 64%).

Effect of Underlying Vasculopathy

Table 2 shows the sensitivity, specificity, PPV, NPV, and accuracy of each calculation technique for the carotid stenosis and nonstenosis groups. There was no significant difference in sensitivity and NPV for most of the calculation techniques between the 2 groups, as shown in Figure 5A and 5D. On the contrary, the specificity, PPV, and accuracy of most calculation methods were lower in the stenosis group (Figure 5B,

5D, and 5E). The differences were most prominent for the TTP method and deconvolution method with the AIF from the contralateral MCA. The first moment and deconvolution methods with the AIF from the PCA and peri-infarct area maintained relatively high specificity in both groups.

Illustrative cases are shown in Figures 6 and 7. As demonstrated, lesion conspicuity was higher for the deconvolution methods, which was a consistent trend noted in all of our cases. The first example (Figure 6) is a case without ICA stenosis in which most of the calculation methods except for deconvolution failed to demonstrate cortical involvement. Note that the images generated by deconvolution methods did not differ significantly with different AIFs, which was a consistent trend noted for those patients without ICA stenosis. The second case (Figure 7) involves a patient who had a balloon occlusion of the right ICA for treatment of a right cavernous giant aneurysm. Her follow-up DWI in 24 hours demonstrated a parietooccipital MCA/PCA watershed infarct (Figure 7b), presumably caused by flow depletion in the right ICA territory. There is a noticeable difference in the extent of perfusion abnormality between the 4 deconvolution methods (Figure 7i, 7j, 7k, and 7l). The deconvolution method with the AIF from the peri-infarct area (Figure 7l) provides the most accurate depiction of the final territory of infarction (Figure 7b). These differences between deconvolution methods were frequently observed for the patients with ICA stenoses.

Discussion

We have shown here that the sensitivity and specificity of the transit time computation methods in visualizing critical hypoperfusion vary significantly, depending on the chosen technique. Because we believe that the main role of PWI is to supplement the relatively low sensitivity of DWI, the calculation methods that have sensitivities lower than or equal to DWI may not be useful for stroke imaging. From this point of view, the optimal computation techniques may include the deconvolution, first moment, and TTP methods, all of which had considerably higher sensitivity compared with DWI. Among these techniques, the deconvolution method had the highest sensitivity values.

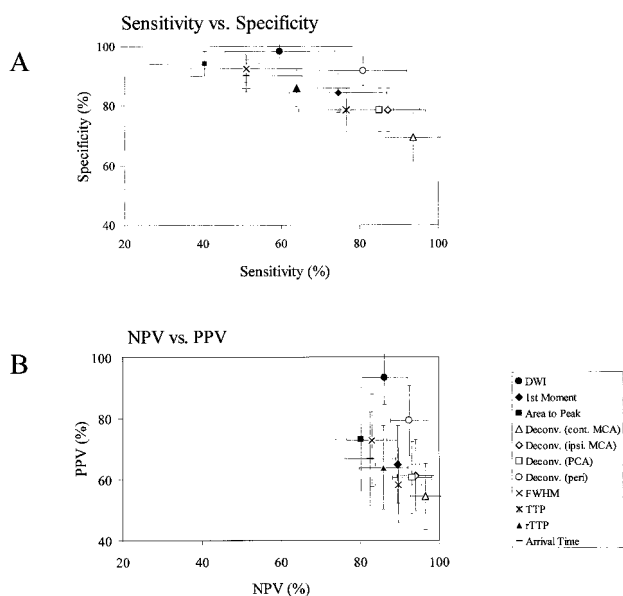


Figure 4. Plots of sensitivity versus specificity (A) and NPV versus PPV (B) for each calculation technique are shown. Data of DWI are also shown as reference. Error bars indicate 95% CIs.

TABLE 2. Sensitivity, Specificity, PPV, NPV, and Accuracy Between Carotid Stenosis and Nonstenosis Groups

	Sensitivity, %		Specificity, %		PPV, %		NPV, %		Accuracy, %	
	Stenosis	Nonstenosis	Stenosis	Nonstenosis	Stenosis	Nonstenosis	Stenosis	Nonstenosis	Stenosis	Nonstenosis
First moment	75 (58-92)	74 (56-92)	80 (70-90)	89 (81-97)	60 (42-78)	71 (53-89)	89 (81-97)	90 (82-98)	79 (70-87)	85 (77-92)
Area to peak	29 (11-47)	52 (32-73)	97 (92-100)	92 (85-99)	78 (51-100)	71 (49-92)	77 (68-87)	84 (75-92)	77 (68-86)	81 (73-89)
Deconvolution (contralateral MCA)	96 (88-100)	91 (80-100)	48† (36-61)	90† (83-98)	43† (29-56)	78† (62-93)	97 (90-100)	96 (92-100)	62† (52-72)	90† (84-97)
Deconvolution (ipsilateral MCA)	88 (74-100)	87 (73-100)	68* (57-80)	89* (81-97)	53 (37-68)	74 (58-91)	93 (86-100)	95 (89-100)	74* (64-83)	88* (81-95)
Deconvolution (PCA)	88 (74-100)	83 (67-98)	70* (58-82)	87* (78-95)	54 (38-69)	70 (53-88)	93 (86-100)	93 (86-100)	75 (66-84)	86 (78-93)
Deconvolution (peri-infarct)	79 (63-95)	83 (67-98)	85* (76-94)	98* (95-100)	68* (51-85)	95* (85-100)	91 (84-99)	94 (88-100)	83* (75-91)	94* (89-99)
FWHM	50 (30-70)	52 (32-73)	88 (80-96)	97 (92-100)	63 (41-85)	86 (67-100)	82 (72-91)	84 (76-93)	77 (68-86)	85 (77-92)
TTP	79 (63-95)	74 (56-92)	58† (46-71)	98† (95-100)	43† (29-58)	94† (84-100)	88 (77-98)	91 (84-98)	64† (54-75)	92† (86-98)
rTTP	67 (48-86)	61 (41-81)	82 (72-91)	90 (83-98)	59 (41-78)	70 (50-90)	86 (77-95)	86 (77-94)	77 (68-86)	82 (74-90)
Arrival time	67* (48-85)	35* (14-55)	85 (80-90)	95 (88-100)	64 (37-91)	73 (51-94)	86 (77-96)	79 (71-88)	80 (71-89)	79 (70-87)

Numbers in parentheses are the 95% CI.

*Statistically significant difference between stenosis and nonstenosis groups ($P < 0.05$); †statistically significant difference between stenosis and nonstenosis groups ($P < 0.005$).

The inferior sensitivity of the first moment method compared with the deconvolution method was an anticipated result from the model described by Weisskoff et al.²⁶ Their model has shown that the MTT calculated by the first moment of the concentration-time curve will in some cases be underestimated by a factor of 2. The first moment method is based on the indicator-dilution theory used for the measurement of flow through an organ or tissue.²⁷ After injection of an indicator such as dye, ice water, or radioactive tracers proximal to the target organ, the indicator concentration distal to the organ is measured. The first moment of the measured efflux concentration-time curve is the MTT of the organ. In tomographic perfusion imaging, however, the measured concentration-time curve of a pixel in the brain is not the distribution of transit time. At best, we can measure the total

amount of the original bolus that remains in the tissue. Thus, the first moment method is not the MTT when used for cross-sectional imaging.²⁶ The deconvolution method, on the other hand, is able to assess the true MTT,^{20,21} and this may have been part of the reason for the outstandingly high lesion conspicuity of the deconvolution method, as demonstrated in Figures 6 and 7.

Our study has shown that underlying vasculopathy in the ICA >70% is another factor that may significantly influence the results of perfusion imaging, which is in agreement with the previous report by Neumann-Haefelin et al.²⁸ Their report had shown that the perfusion maps of those patients with steno-occlusive disease tended to overestimate the area that eventually evolve into infarct.²⁸ Our study has shown the specificity of the transit time maps to be inferior for those

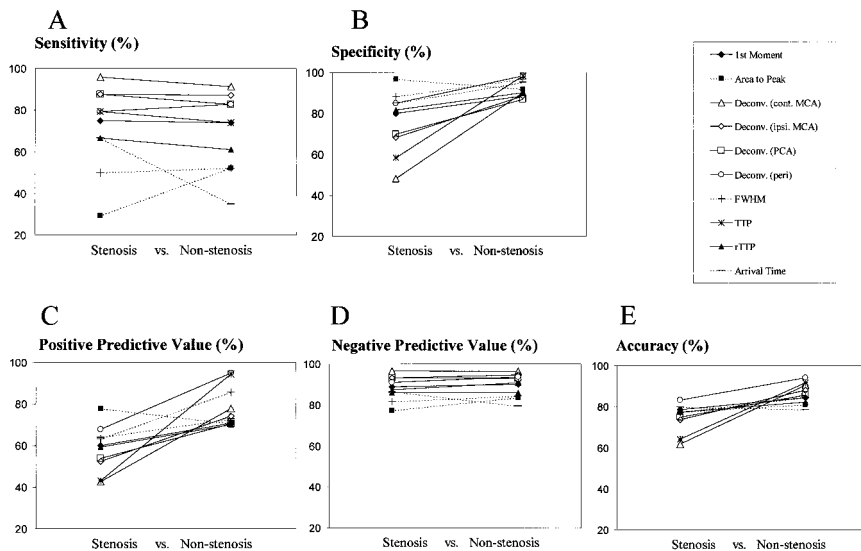


Figure 5. Graphs show difference of sensitivity (A), specificity (B), PPV (C), NPV (D), and accuracy (E) between ICA stenosis and nonstenosis groups. Sensitivity and NPV of most of the techniques did not differ significantly between the 2 groups. Specificity, PPV, and accuracy were lower in the stenosis group for most of the calculation methods. Note that the calculation methods such as in TTP and deconvolution method with AIF from contralateral MCA had significantly lower values when vasculopathy was present.

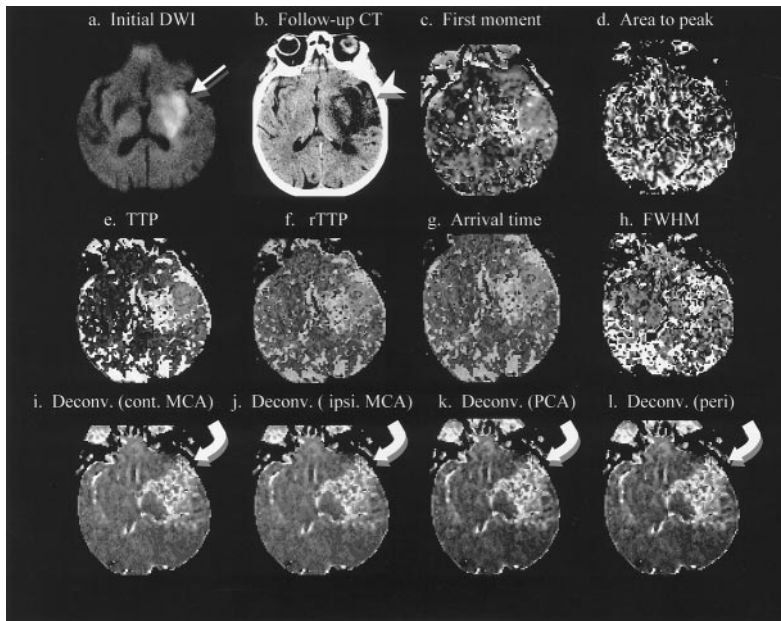


Figure 6. This 80-year-old woman presented with acute onset of aphasia and confusion. Initial DWI (a) showed an area of abnormality involving the left basal ganglia (arrow), which was later shown to be an infarct also involving the anterior temporal cortex (arrowhead) on follow-up CT (b). PWI at the time of onset using the first moment (c), time to peak (e), and relative time to peak (f) images demonstrated an area of abnormal perfusion in the left basal ganglia, but the cortical involvement was missed with these techniques. The deconvolution method (Deconv.; i through l) was the only calculation technique that showed an unequivocal area of cortical involvement in the anterior temporal MCA territory (curved arrows). Cont. indicates contralateral; ipsi, ipsilateral; and peri, peri-infarction arteries.

cases with ICA stenosis >70%, which in turn indicates that there were higher incidence of false-positive areas depicted by these perfusion maps. Both the study of Neumann-Haefelin et al²⁸ and our study indicate that there may be some limitation in the perfusion imaging when assessing patients with steno-occlusive disease. The steno-occlusive disease at the parent artery may cause distortion of the concentration-time curve as a result of turbulent flow at the stenotic segment of the vessel or longer path through the collateral arteries. We hypothesized that the transit time images calculated from the distorted curves may lead to failure in accurately demonstrating the local perfusion abnormality, which was shown to be true.

The effect of steno-occlusive vascular disease was more prominent for certain calculation methods, such as the TTP

method. TTP is a simple measure of perfusion that calculates the time it takes the bolus of contrast to reach its maximum concentration in a given region of brain. This simple parameter is straightforward to compute and thus has become widely popular in clinical practice.^{13,22-24} Despite such benefits, this technique was shown to be highly vulnerable to steno-occlusive disease and can be concluded to be less reliable in the presence of steno-occlusive vascular disease. A threshold method proposed for this TTP method may be useful to increase the accuracy of the imaging technique.²⁸

Some of the deconvolution methods were also vulnerable to the presence of steno-occlusive disease, which may have been caused by the misrepresentation of the selected AIF for the flow at the affected area of the brain. Although it is ideal to analyze each pixel with the AIF of its own feeding artery,

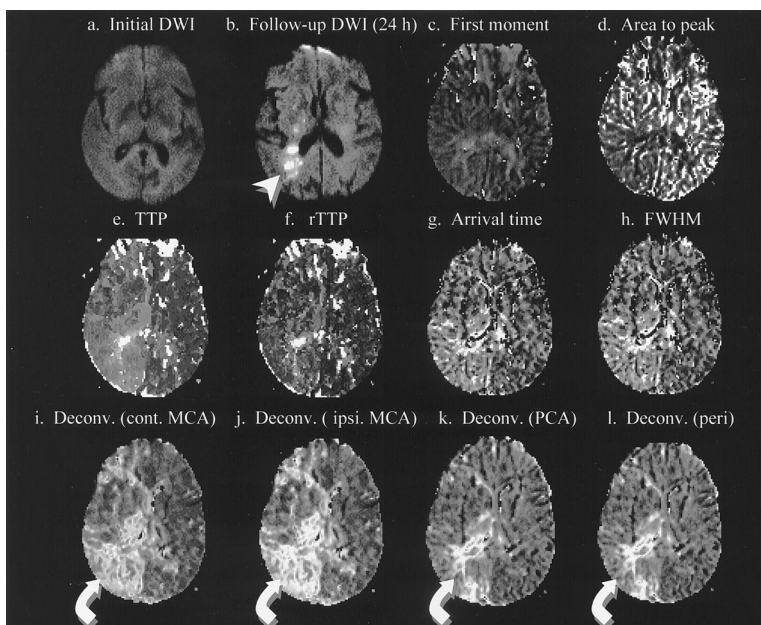


Figure 7. This 80-year-old woman was admitted to hospital for balloon occlusion of a right cavernous carotid aneurysm. The patient remained asymptomatic until she developed a left facial droop during the evening after the procedure. Her initial DWI was negative for an infarct (a). On the follow-up DWI in 24 hours (b), the lesion in the parietooccipital region at the MCA/PCA watershed zone became apparent (arrowhead). PWIs using deconvolution methods (Deconv.; i through l) revealed abnormality involving the right posterior MCA/PCA watershed (curved arrows), whereas the other methods failed to demonstrate an unequivocal area of abnormality (c through h). Note that the extent of abnormality demonstrated on the deconvolution methods differs, depending on the selected AIFs. The image calculated by the AIF from the contralateral MCA (j) overestimates the area of infarction, whereas the images with the AIF from the peri-infarction area (l) showed the closest agreement with the follow-up DWI (b). Abbreviations as in Figure 6.

this is not clinically feasible because a large number of AIFs will be required. Thus, an AIF is typically chosen from a single location, such as the ICA or MCA contralateral to the side of infarct.^{20,21,29} In the evaluation of a patient with steno-occlusive disease, however, the AIF chosen from the contralateral vessel may not represent the AIF of the ipsilateral hemisphere, where there may be significant curve distortion. The resultant MTT images will tend to overestimate the region of abnormal flow, resulting in lower specificity. Conversely, when the AIF is chosen from the peri-infarct arteries, higher specificity to the local flow disturbances is obtained, because the AIF corrects for the contrast delay and dispersion that occur distal to the vascular stenosis. Thus, in the presence of steno-occlusive disease, selection of AIF from the peri-infarct artery is one of the techniques of choice to delineate the areas with true MTT prolongation.

Although proven a robust technique, a disadvantage of the deconvolution method may be the mandatory extra step of human input, namely the selection of an AIF from the source images. Compared with the other methods, which can be fully automated, this human-dependent extra step could be somewhat problematic in an acute clinical setting. However, the AIF selection procedure is fairly straightforward and takes <2 to 3 minutes by a trained person. In our experience, the interobserver difference in the shape of the AIF and the quality of the calculated perfusion maps are extremely low; thus, we believe that the technique is feasible. Fully automated selection of AIF has also been proposed.²⁹ In addition, the total computation time is <15 minutes, including the selection of AIF, which we believe is within an acceptable time frame.

The findings reported here should be viewed in the context of several methodological limitations. First, the number of patients in our study is limited. More subjects may be necessary to draw a solid conclusion regarding the best calculation methods of choice. Second, the 2 subgroups analyzed in our study were not perfectly matched for potentially confounding factors, such as cerebral risk factors and time between symptom onset and MRI. These may have had an influence on the study results. Third, not all the follow-up images were MR; CT scans also were included. Ideally, one modality is to be used for a gold standard, with MR being the superior choice with higher lesion conspicuity. However, there is no question that the CT is an alternative follow-up method with satisfactory lesion conspicuity, and we believe that it is a suitable modality as a gold standard. Fourth, we used the final area of infarct on the follow-up studies as the gold standard for evaluating the transit time images. However, a direct correlation between transit time abnormality and infarction is yet to be proven; thus, the ideal gold standard of the transit time images may have been another well-established perfusion imaging technique, such as PET, SPECT, or xenon CT. In an acute stroke setting, however, it is not always possible to obtain multiple different studies for perfusion assessment. Furthermore, because our goal was to assess the trends and limitation of various transit time calculation methods that are currently in use for stroke imaging, we believe that it is clinically relevant to use the final area of infarct as the gold standard.

In conclusion, we have shown that both the calculation technique and the presence of underlying vasculopathy have direct impact on the results of PWI. Calculation techniques with high sensitivity even in the presence of steno-occlusive disease were the first moment method and deconvolution method with the AIF selected from the peri-infarct arteries. The higher lesion conspicuity of the deconvolution method compared with the other calculation techniques leads us to conclude that this is considered to be one of the best methods of choice for stroke imaging.

Acknowledgments

This work was supported in part by an International Investigator's Award from the Japanese Society of Magnetic Resonance in Medicine and a research grant from the Brain Science Foundation, both given to Dr Yamada. We express our gratitude to David A. Shrier, MD, and Amy C. Sievers, MM, for invaluable help in reviewing the manuscript.

References

1. Sorensen AG, Buonanno FS, Gonzalez RG, Schwamm LH, Lev MH, Huang-Hellinger FR, Reese TG, Weisskoff RM, Davis TL, Suwanwela N, Can U, Moreira JA, Copen WA, Look RB, Finklestein SP, Rosen BR, Koroshetz WJ. Hyperacute stroke: evaluation with combined multisection diffusion-weighted and hemodynamically weighted echo-planar MR imaging. *Radiology*. 1996;199:391–401.
2. Sorensen AG, Copen WA, Østergaard L, Buonanno FS, Gonzalez RG, Rordorf G, Rosen BR, Schwamm LH, Weisskoff RM, Koroshetz WJ. Hyperacute stroke: simultaneous measurement of relative cerebral blood volume, relative cerebral blood flow, and mean tissue transit time. *Radiology*. 1999;210:519–527.
3. Rordorf G, Koroshetz WJ, Copen WA, Gonzalez G, Yamada K, Schaefer PW, Schwamm LH, Ogilvy CS, Sorensen AG. Diffusion- and perfusion-weighted imaging in vasospasm after subarachnoid hemorrhage. *Stroke*. 1999;30:599–605.
4. Rosen BR, Belliveau JW, Vevea JM, Brady TJ. Perfusion imaging with NMR contrast agents. *Magn Reson Med*. 1990;14:249–265.
5. Rosen BR, Belliveau JW, Aronen HJ, Kennedy D, Buchbinder BR, Fischman A, Gruber M, Glas J, Weisskoff RM, Cohen MS. Susceptibility contrast imaging of cerebral blood volume: human experience. *Magn Reson Med*. 1991;22:293–299.
6. Baird AE, Warach S. Magnetic resonance imaging of acute stroke. *J Cereb Blood Flow Metab*. 1998;18:583–609.
7. Warach S, Dashe JF, Edelman RR. Clinical outcome in ischemic stroke predicted by early diffusion-weighted and perfusion magnetic resonance imaging: a preliminary analysis. *J Cereb Blood Flow Metab*. 1996;16:53–59.
8. Guckel FJ, Brix G, Schmiedek P, Piepgras Z, Becker G, Kopke J, Gross H, Georgi M. Cerebrovascular reserve capacity in patients with occlusive cerebrovascular disease: assessment with dynamic susceptibility contrast enhanced MR imaging and the acetazolamide stimulation test. *Radiology*. 1996;201:405–412.
9. Karonen JO, Vanninen RL, Liu Y, Østergaard L, Kuikka JT, Nuutinen J, Vanninen EJ, Partanen PLK, Vainio PA, Korhonen K, Perkiö J, Roivainen R, Sivenius J, Aronen HJ. Combined diffusion and perfusion MRI with correlation to single-photon emission CT in acute ischemic stroke: ischemic penumbra predicts infarct growth. *Stroke*. 1999;30:1583–1590.
10. Gibbs JM, Wise RJ, Leenders KL, Jones T. Evaluation of cerebral perfusion reserve in patients with carotid-artery occlusion. *Lancet*. 1984;1:310–314.
11. Sette G, Baron JC, Mazoyer B, Levasseur M, Pappata S, Crouzel C. Local brain hemodynamics and oxygen metabolism in cerebrovascular disease. *Brain*. 1989;112:931–951.
12. Darby DG, Barber PA, Gerraty RP, Desmond PM, Yang Q, Parsons M, Li T, Tress BM, Davis SM. Pathophysiological topography of acute ischemia by combined diffusion-weighted and perfusion MRI. *Stroke*. 1999;30:2043–2052.
13. Neumann-Haefelin T, Wittsack HJ, Wenserski F, Siebler M, Seitz RJ, Mödder U, Freund HJ. Diffusion- and perfusion-weighted MRI: the DWI/PWI mismatch region in acute stroke. *Stroke*. 1999;30:1591–1597.

14. Roberts TPL, Vexler Z, Derugin ME, Moseley ME, Kucharczyk J. High-speed MR imaging of ischemic brain injury following stenosis of middle cerebral artery. *J Cereb Blood Flow Metab*. 1993;13:940-946.
15. Zierler KL. Equations for measuring blood flow by external monitoring of radioisotopes. *Circ Res*. 1965;16:309-321.
16. Axel L. Cerebral blood flow determination by rapid-sequence computed tomography. *Radiology*. 1980;137:679-686.
17. Nighoghossian N, Berthezene Y, Philippon B, Adeleine P, Froment JC, Trouillas P. Hemodynamic parameter assessment with dynamic susceptibility contrast magnetic resonance imaging in unilateral symptomatic internal carotid artery occlusion. *Stroke*. 1996;27:474-479.
18. Gobbel GT, Cann CE, Fike JR. Measurement of regional cerebral blood flow using ultrafast computed tomography. *Stroke*. 1991;22:768-771.
19. Tzika AA, Massoth RJ, Ball WS Jr, Majumdar S, Dunn RS, Kirks DR. Cerebral perfusion in children: detection with dynamic contrast-enhanced T2*-weighted MR images. *Radiology*. 1993;187:449-458.
20. Østergaard L, Weisskoff RM, Chesler DA, Glydensted C, Rosen RB. High resolution measurement of cerebral blood flow using tracer bolus passages, part I: mathematical approach and statistical analysis. *Magn Reson Med*. 1996;36:715-725.
21. Østergaard L, Sorensen AG, Kwong KK, Weisskoff RM, Glydensted C, Rosen BR. High resolution measurement of cerebral blood flow using tracer bolus passages, part II: experimental comparison and preliminary results. *Magn Reson Med*. 1996;36:726-736.
22. Tsuchiya K, Inaoka S, Mizutani Y, Hachiya J. Echo-planar perfusion MR of moyamoya disease. *Am J Neuroradiol*. 1998;19:211-216.
23. Sunshine JL, Tarr RW, Lanzieri CF, Landis DM, Selman WR, Lewin JS. Hyperacute stroke: ultrafast MR imaging to triage patients prior to therapy. *Radiology*. 1999;212:325-332.
24. Kluytmans M, van der Grond J, Viergever MA. Gray matter and white matter perfusion imaging in patients with severe carotid artery lesions. *Radiology*. 1998;209:675-682.
25. Stewart GN. Researches on the circulation time in organs and on the influences which effect it, parts I through III. *J Physiol* 1894;15:1-89.
26. Weisskoff RM, Chesler D, Boxerman JL, Rosen BR. Pitfalls in MR measurement of tissue blood flow with intravascular tracers: which mean transit time? *Magn Reson Med*. 1993;29:553-559.
27. Meier P, Zierler KL. On the theory of the indicator-dilution method for measurement of blood flow and volume. *J Appl Physiol*. 1954;6:731-744.
28. Neumann-Haefelin T, Wittsack HJ, Fink GR, Wenserski F, Li TQ, Seitz RJ, Siebler M, Modder U, Freund HJ. Diffusion- and perfusion-weighted MRI. influence of severe carotid artery stenosis on the DWI/PWI mismatch in acute stroke. *Stroke*. 2000;31:1311-1317.
29. Rempp KA, Brix G, Wenz F, Becker CR, Guckel F, Lorenz WJ. Quantification of regional cerebral blood flow and volume with dynamic susceptibility contrast-enhanced MR imaging. *Radiology*. 1994;193:637-641.